

Observation of Altermagnetic Order Switching in Bulk MnTe by Polarized Neutron Diffraction

Zheyuan Liu,¹ Shinichiro Asai,¹ Shingo Takahashi,¹ Hiraku Saito,¹ Taro Nakajima,^{1,2,3} and Takatsugu Masuda^{1,3,4}

¹*Institute for Solid State Physics, the University of Tokyo, Kashiwa 277-8581, Japan*

²*RIKEN Center for Emergent Matter Science (CEMS), Saitama 351-0198, Japan*

³*Institute of Materials Structure Science, High Energy Accelerator Research Organization, Ibaraki 305-0801, Japan*

⁴*Trans-scale Quantum Science Institute, the University of Tokyo, Tokyo 113-0033, Japan*

(Dated: May 22, 2026)

Altermagnetic order, characterized by the Néel vector, breaks time-reversal symmetry (TRS) even in the nonrelativistic limit. Although spin-polarized and anomalous transport phenomena emerge with this order, they are mutually compensated by TRS-connected antiphase domains with opposite Néel vectors. Here we employ polarized neutron diffraction to directly probe the altermagnetic order in MnTe. Pronounced nuclear-magnetic interference terms were observed, providing direct evidence of a net Néel vector in the bulk crystal. Moreover, a weak ferromagnetic moment (WFM), originating from relativistic spin-orbit coupling, was found to be coupled with the altermagnetic order. Both the altermagnetic order and the WFM can be switched by milli-Tesla-scale magnetic field cooling.

Breaking time-reversal symmetry (TRS) in magnetic materials enables efficient spin-charge conversion [1–6], underpinning their spintronic functionalities. Recent classification based on spin-group symmetry identified a new class of TRS-breaking magnets [7–9], dubbed altermagnets, which are promising material for generating giant spin current under stray-field-free condition. A range of exotic phenomena has been experimentally verified in altermagnets, including spin-split electronic bands [10–16], chiral-split magnon band [17, 18], anomalous Hall effect (AHE) [14, 19–23], and other experimental signatures of TRS-breaking [24, 25]. These properties inherently rely on altermagnetic order, thus only emerge when the distribution of altermagnetic antiphase domains is imbalanced in real materials. In the absence of net magnetization, whether the altermagnetic order can be directly controlled by external magnetic fields remains a crucial challenge on the pathway to functional altermagnetic devices.

The minimal model of altermagnetism consists of antiferromagnetically arranged electron spins embedded in a nonmagnetic atomic or orbital environment with rotational symmetry [26, 27]. In the presence of additional effects such as spin-orbit coupling (SOC) [28–32], lattice defect or distortion [33–35], and strain [25, 36–38], the degeneracy between altermagnetic antiphase domain states can be lifted by external magnetic fields in contrast with conventional antiferromagnets. SOC activates staggered Dzyaloshinskii-Moriya (DM) interactions in altermagnets, giving rise to a weak ferromagnetic moment (WFM) coupled to the altermagnetic order by spin canting [14, 20, 30, 39]. Anisotropic g -tensors with rotational symmetries lead to the WFM originating from orbital magnetization [32, 40, 41]. Early studies showed that the altermagnetic antiphase domains in MnF₂ were selected by field cooling [33, 34], likely due to lattice defects. Moreover, chemical doping induces WFM in MnF₂ via lattice distortion [35]. Piezomagnetic effect in altermagnets induces or enhances WFM as well [25, 36–38],

suggesting the possible domain selection by combined application of external strain and magnetic fields.

Antiphase domain states in conventional collinear antiferromagnets are identical in the reciprocal space when SOC is absent, and are thus only detectable in the real space. By contrast, due to TRS breaking, antiphase domain states in altermagnets are distinguishable even in reciprocal space [33, 34, 42–45]. For neutrons scattered by both the ordered electron spins and nuclear ligands in altermagnets, the observable manifests itself as nuclear-magnetic interference (NMI) terms, which alter their sign between antiphase domain states. The sign change reflects the distinguishability of time-reversal-related antiphase domains in reciprocal space, which is a defining property of altermagnets. In contrast, in conventional collinear antiferromagnets where opposite-spin sublattices are connected by time reversal combined with translation or inversion, such NMI signals are not expected, as rigorously demonstrated in Ref. [42]. The NMI effect was conventionally utilized for an accurate measurement of the magnetic moment distribution in ferromagnets [46] because it amplifies the detection on faint magnetic moments down to the $10^{-3}\mu_{\text{B}}/\text{atom}$ scale [47]. In early polarized neutron diffraction (PoND) experiments, the NMI term was observed in magnets which are currently classified as altermagnets [33, 34, 43, 44], whose magnitude is comparable to that of nuclear and magnetic diffraction. Here, by performing PoND on the altermagnetic prototype MnTe, we observed pronounced NMI terms, representing a direct probe of the altermagnetic order in altermagnet. The switching of altermagnetic order, along with the WFM in MnTe, was realized by milli-Tesla-scale magnetic-field cooling.

MnTe has been confirmed as a prototype altermagnet by photoemission spectroscopy [10–12] and inelastic neutron scattering [17] in recent studies. MnTe crystallizes in a centrosymmetric hexagonal lattice with space group $P6_3/mmc$ [48], and no change in the lattice symmetry has been reported across the Néel temperature

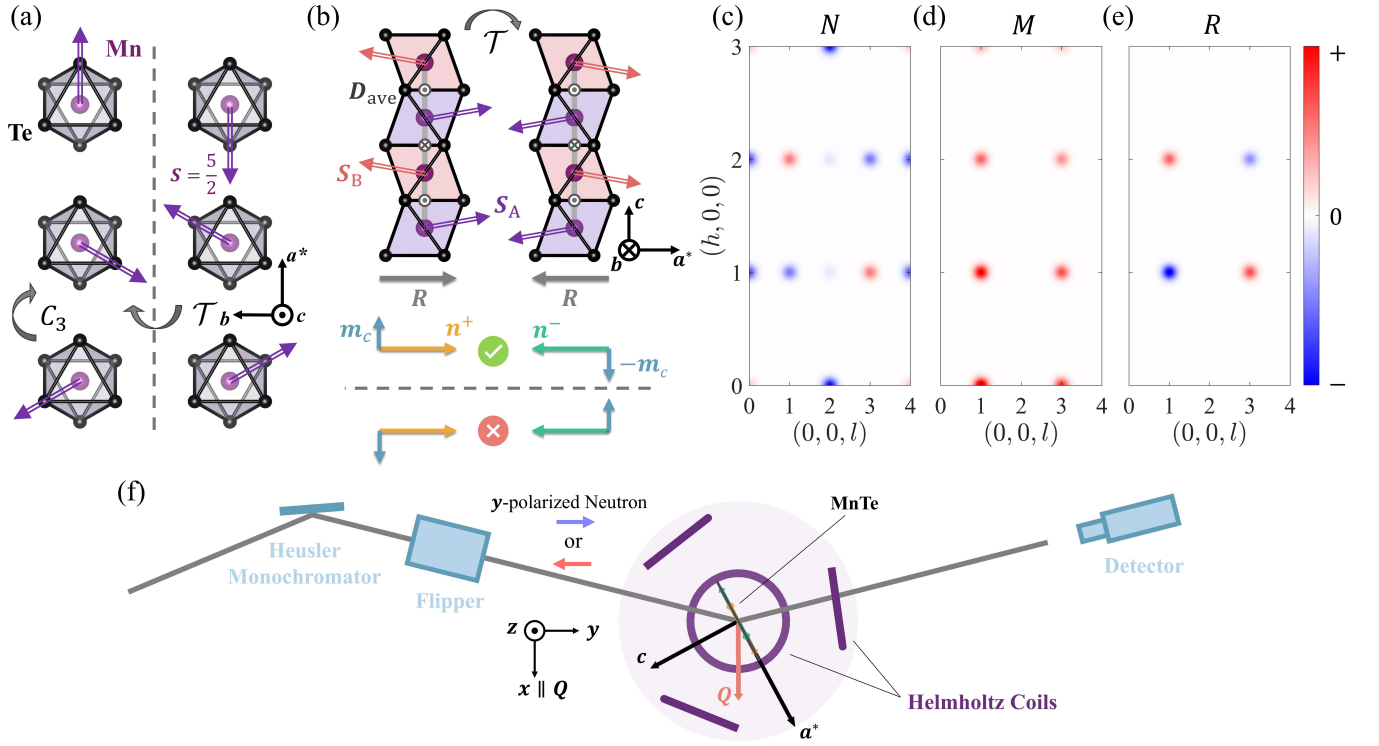


FIG. 1. (a) Six altermagnetic domain states schematically shown for MnTe. The columns show orientational domain states related by a C_3 rotation, and the rows show antiphase domain states related by time reversal \mathcal{T} . (b) Two antiphase domain states (upper panel) with Néel vectors \mathbf{n}^+ and \mathbf{n}^- parallel to the a^* -axis. The NMI vector \mathbf{R} aligns with the Néel vector and thus changes sign between the antiphase domain states. Spins are canted due to the alternating averaged DM vector \mathbf{D}_{ave} , leading to a finite net moment \mathbf{m}_c . The canting angle is exaggerated for illustration. The spin configuration in the lower panel is forbidden. Calculated structure factors of (c) nuclei, (d) spins, and (e) the scalar part of the NMI vector in the $(h0l)$ plane. (f) Schematic of the PoND experimental setup in the half-polarized mode. The incident beam is polarized, while the final beam is not analyzed. A pair of vertical and three horizontal Helmholtz coils are installed at the sample position to generate the guide field as well as the cooling field along arbitrary directions.

T_N [49]. Below T_N , an A -type antiferromagnetic ground state with spins oriented along the $\langle 1\bar{1}0 \rangle$ direction is realized in MnTe [24, 25]. Two types of magnetic domain states coexist: the orientational domain states related by the C_3 lattice symmetry and the antiphase domain states connected by TRS, as shown in Fig. 1(a). In the centrosymmetric lattice of MnTe, the local DM interactions are compensated in the unit cell. However, in the presence of SOC, the feedback from altermagnetic order on the charge distribution lowers the lattice symmetry, allowing an uncompensated DM interaction which connects the adjacent Mn layers [29]. This DM interaction can be understood, at the level of general symmetry considerations, as an effective four-spin interaction [50, 51]. The averaged interlayer DM vector, \mathbf{D}_{ave} , lies perpendicular to the Néel vector, $\mathbf{n} = \mathbf{S}_A - \mathbf{S}_B$, and alternates along the c -axis, resulting in a canted moment, $\mathbf{m}_c = \mathbf{S}_A + \mathbf{S}_B$, aligned with the c -axis (see Section V in Supplemental Material (SM) [52] for details). The vector \mathbf{D}_{ave} ensures that the opposite \mathbf{m}_c corresponds to the opposite \mathbf{n} , as shown in the upper panel of Fig. 1(b), and forbids the spin configuration in the lower panel. A

route for achieving a single magnetic domain in MnTe is to utilize the spin-flop transition [58] and the flipping of WFM. The WFM in MnTe is around $10^{-5} \mu_B/\text{Mn}$ along the c -axis [20], producing almost negligible stray fields (10^{-3} mT, typically 10 mT in ferromagnetic devices), yet enabling the selection of antiphase domain states by external fields. In addition, antiphase domain states in the thin film MnTe were shown to be selected by field cooling along the c -axis [24, 59].

The susceptibility and spontaneous magnetization were measured on bulk MnTe single crystals as a preliminary step toward demonstrating magnetic domain selection by PoND. Figs. 2(a)-2(e) show schematics of Néel vectors selected by external magnetic fields. As shown in Fig. 2(f), below $T_N = 307$ K, the susceptibility along the b -axis after 5-T field cooling (FC), χ_b^{FC} , deviates from that after zero-field cooling (ZFC), χ_b^{ZFC} , and approaches that along the c -axis, χ_c . This indicates a change from χ_{\parallel} to χ_{\perp} , corresponding to an enhanced population of the single orientational domain state shown in Fig. 2(b). The spontaneous WFM, m_c^{spon} , was observed after FC and was found to align with the cooling field direction, as

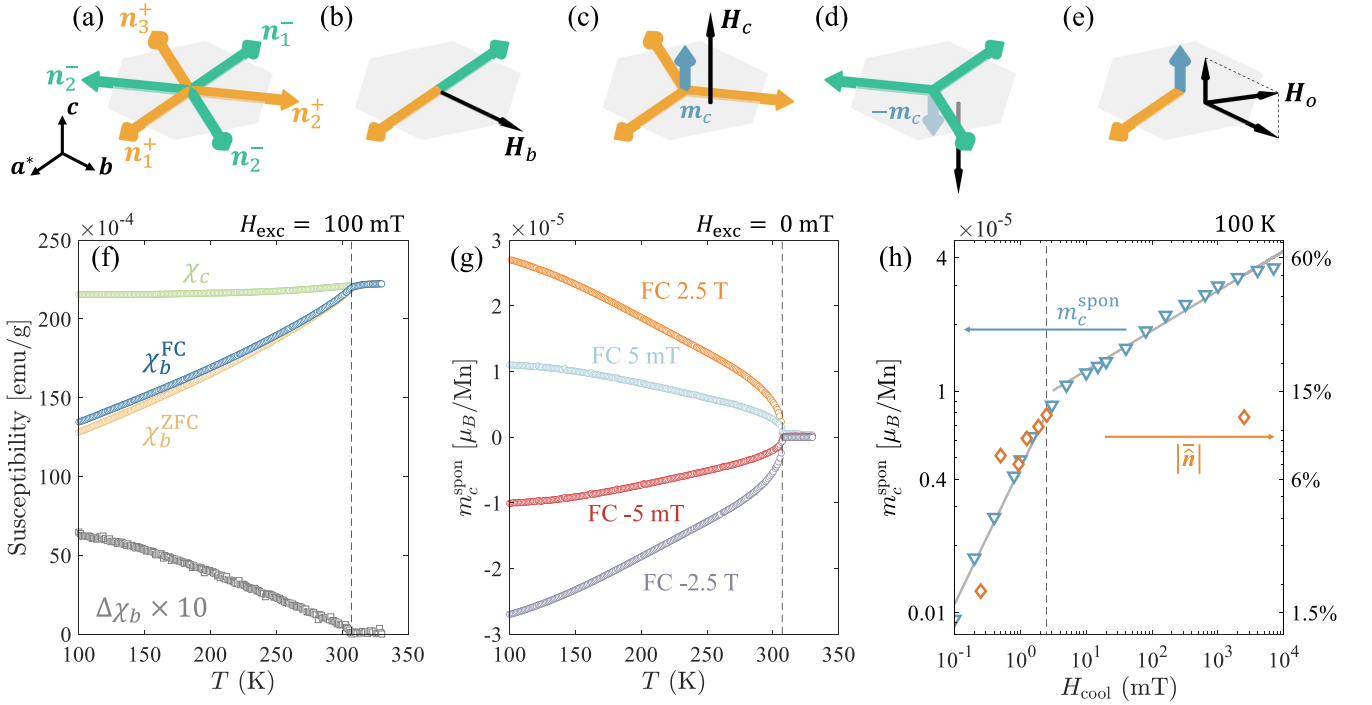


FIG. 2. Schematics of (a) a multi-domain state in zero field, (b) a set of orientational domain states selected by an in-plane field H_b , (c), (d) Sets of antiphase domain states selected by an out-of-plane field H_c , and (e) a single-domain state selected by an oblique field H_o . (f) Magnetic susceptibilities of MnTe along the c -axis (χ_c , green), along the b -axis after ZFC (χ_b^{ZFC} , yellow), and along the b -axis after 5 T FC (χ_b^{FC} , blue). The difference $\Delta\chi_b = \chi_b^{\text{FC}} - \chi_b^{\text{ZFC}}$ is scaled up by a factor of 10 and shown in gray. (g) Spontaneous WFM along the c -axis, m_c^{spon} , in MnTe. The excitation field during the measurement (H_{exc}) was zero. The data were collected upon warming. (h) Cooling-field dependence of m_c^{spon} (blue) and $|\tilde{\mathbf{n}}|$ (orange) at 100 K, shown on a double-logarithmic scale. The gray solid lines are guides for the eye. The dashed line indicates $H_{\text{cool}} = 2.5$ mT.

shown in Fig. 2(g). The magnitude is around $2 \times 10^{-5} \mu_B$ per Mn, consistent with the previous measurements [20]. The ratio of uncompensated DM interactions to the corresponding exchange interaction was estimated from the observed m_c^{spon} to be on the order of 10^{-5} scale (see Section V in SM [52]), supporting interpretation of WFM as a high-order SOC effect as proposed by Ref. [29].

The sign of WFM is switchable by the directions of magnetic fields, suggesting the selection of antiphase domain states as shown in Figs. 2(c) and 2(d). An oblique field in the bc -plane was found to favor a single Néel vector perpendicular to it, as shown in Fig. 2(e), which was indicated by the magnetic measurements after oblique-field cooling (OFC) as well (see Section II in SM [52]). The spontaneous WFM is induced by a cooling field at the milli-Tesla scale and tends to saturate at higher fields, as shown in Fig. 2(h).

Here, referring to the nuclear and magnetic structure factors as N and M , we define a vector quantity $\mathbf{R} = (NM^\dagger + MN^\dagger)$ as a quantitative measure of the NMI effect, whose direction is aligned with \mathbf{M} and whose modulus reflects the interference amplitude. In MnTe, the NMI effect happens where the nuclear Bragg peaks coincide with magnetic Bragg peaks, as shown in

Figs. 1(c)-1(e). Considering the collinear antiferromagnetic spin structure, the NMI vector of MnTe is expressed as

$$\mathbf{R} = \hat{\mathbf{n}}(NM^\dagger + MN^\dagger), \quad (1)$$

where $\hat{\mathbf{n}}$ is the unit Néel vector (see Section VI in SM [52] for details). In a real MnTe sample with six magnetic domains, the components of \mathbf{R} are expressed as

$$R_\alpha = \left[\left(\sum_{\substack{i=1,2,3 \\ s=+,-}} p_i^s \hat{\mathbf{n}}_i^s \right) \cdot \hat{\boldsymbol{\alpha}} \right] R, \quad (\alpha = x, y, z) \quad (2)$$

where p_i^s is the domain population, $\hat{\mathbf{n}}_i^s$ is the unit Néel vector of each domain state, and i and s denote the orientational and antiphase domain states, respectively. Here, a Blume-Maleev coordinate system is adopted, where \mathbf{x} is parallel to the momentum transfer \mathbf{Q} and $\mathbf{y} \perp \mathbf{x}$ in the scattering plane, as shown in Fig. 1(f). Therefore, R_α is a direct manifestation of the net unit Néel vector $\tilde{\mathbf{n}} = \sum_{s=+,-} \sum_{i=1,2,3} p_i^s \hat{\mathbf{n}}_i^s$ in the sample. For an ideal single domain, the modulus $|\tilde{\mathbf{n}}| = 1$. Note that a balanced distribution of antiphase domains always results in $|\tilde{\mathbf{n}}| = 0$,

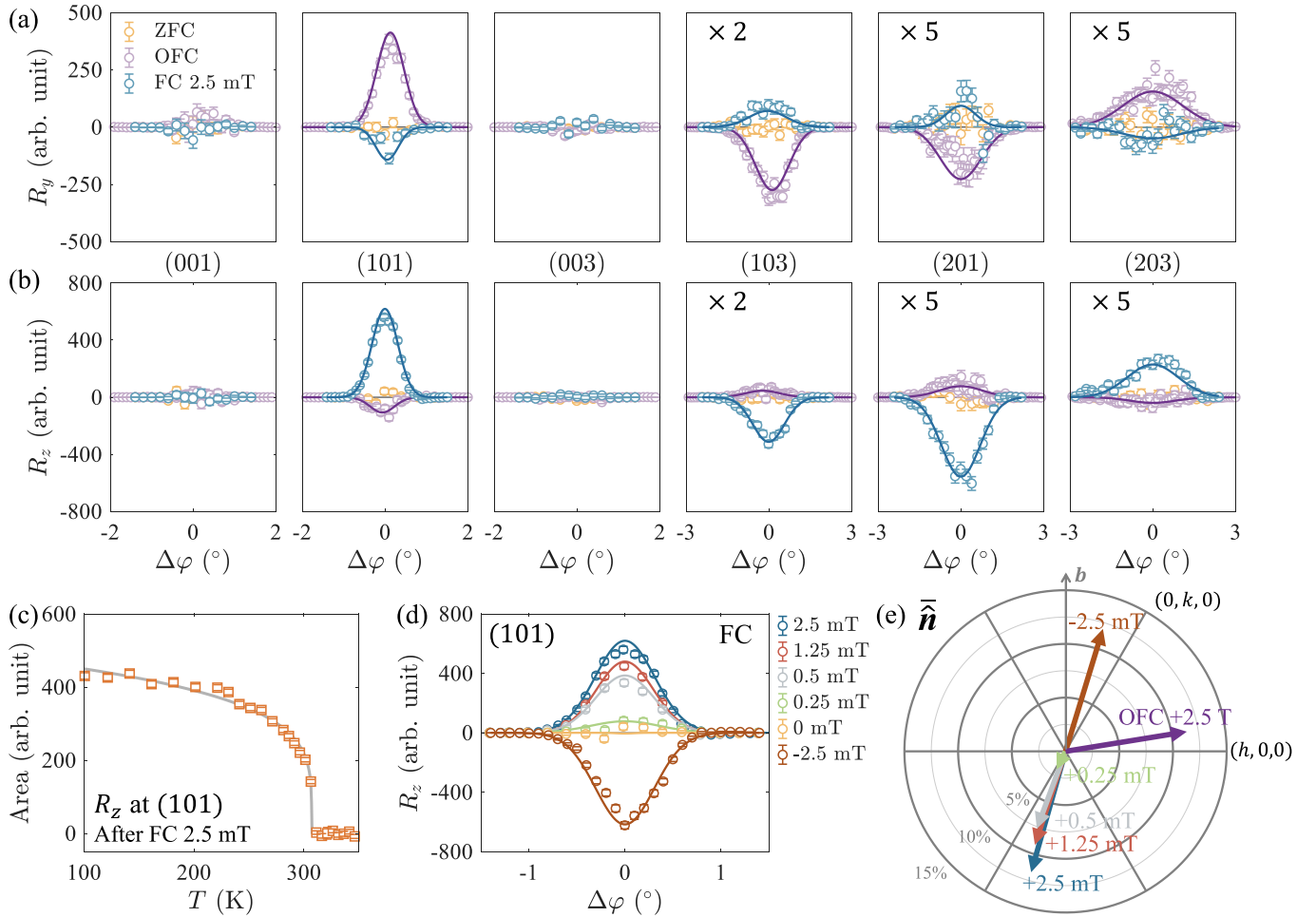


FIG. 3. Components of the NMI vector, (a) R_y and (b) R_z , measured after ZFC, OFC, and FC at the Bragg peaks (001), (101), (003), (103), (201), and (203) at 100 K. Gaussian fits with areas fixed to the calculated values are shown as solid lines. The field in OFC setup was applied in the bc -plane as shown in Fig. 2(e), and the field in FC setup was applied in the c -axis. (c) Temperature dependence of R_z at (101) after 2.5 mT FC. A power-law fit is shown as a solid line. (d) Cooling-field dependence of R_z at (101) at 100 K. (e) Mapping of \bar{n} after each cooling condition in the ab -plane. The different orientations of \bar{n} in the FC and OFC setups result in opposite signs of R_y in (a) and R_z in (b).

leading to zero R_α . When the net unit Néel vector is nonzero, the NMI effect causes a variation in the intensities of scattered neutrons depending on the incident polarization direction, up or down. In particular, when the polarization axis of the incident neutrons is parallel to the y (z) direction, the difference between the intensities measured with up- and down-incident polarization is proportional to R_y (R_z) (see Section III in SM [52]). However, neutrons do not probe the magnetic moment parallel to \mathbf{Q} (the x -direction), and therefore R_x cannot be measured.

To probe the altermagnetic order, the PoND experiments were performed on MnTe single crystals in the $(h0l)$ scattering plane using a triple-axis spectrometer. Milli-Tesla-scale magnetic fields in arbitrary directions were generated by a group of Helmholtz coils at the sample position, serving as the guide field for polarized neutrons as well as the cooling field for the sample, as illus-

trated in Fig. 1(f). The components of the NMI vector, R_y and R_z , were unambiguously probed by half-polarized mode at (101), (103), (201), and (203), as shown in Figs. 3(a) and 3(b). Specifically, large R_y and small R_z were observed after OFC (2.5 T along the c -axis and 4.3 T along the b -axis), small R_y and large R_z after FC along the c -axis, and both zero after ZFC. By contrast, R_y and R_z are always zero at (001) and (003). They appear at the superpositions of magnetic and nuclear Bragg peaks with alternating sign, revealing their origin as interference terms, consistent with the calculation in Fig. 1(e). The temperature dependence of R_z shows critical behavior at T_N , as shown in Fig. 3(c), indicating that it contains a magnetic contribution. The sign of R_z is switched by FC with fields in the opposite direction, as shown in Fig. 3(d). The magnitude also decreases as the cooling field decreases.

The net unit Néel vector \bar{n} was obtained from R_y

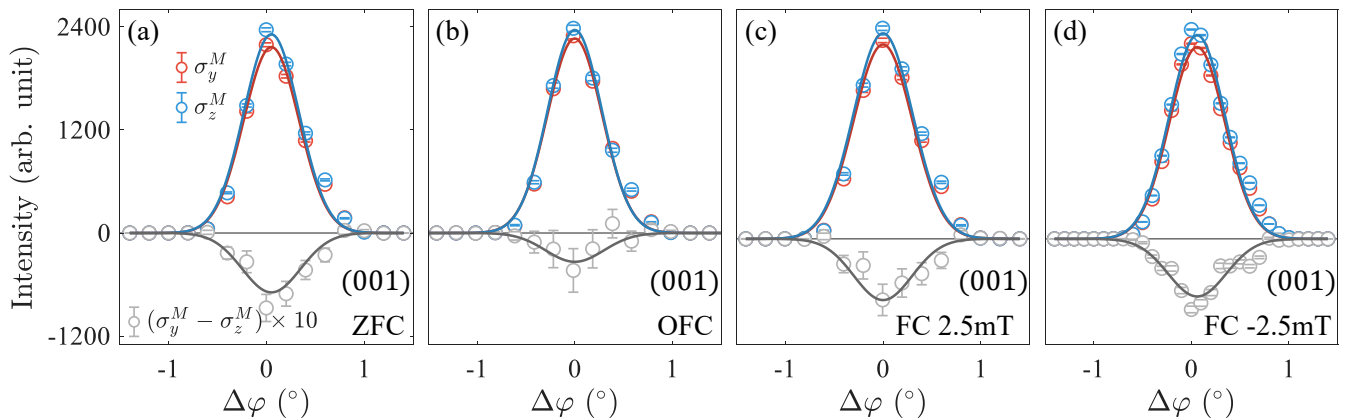


FIG. 4. σ_y^M (red) and σ_z^M (blue) obtained using z -polarization after (a) ZFC, (b) OFC, (c) FC at 2.5 mT, and (d) FC at -2.5 mT at the pure magnetic Bragg peak (001) at 100 K. The difference $\sigma_y^M - \sigma_z^M$ is scaled up by a factor of 10 and shown in gray. Gaussian fits with areas fixed to the calculated values are shown as solid lines.

and R_z and mapped in the ab -plane (see Section VII in SM [52]), as shown in Fig. 3(e). The $\bar{\mathbf{n}}$ vectors reach the same modulus, approximately 12%, after OFC at 2.5 T and FC at ± 2.5 mT. They are not strictly aligned with the crystal axes because of the averaging over multiple domains in the sample (see Section VII in SM [52]). Specifically, after OFC, the $\bar{\mathbf{n}}$ tends to align with the a^* -axis, which is perpendicular to the oblique cooling field in the bc -plane, indicating an enhanced population of the orientational domain state favored by the field component along the b -axis. Despite the relatively small domain imbalance, the $\bar{\mathbf{n}}$ is switched by FC in the opposite direction along the c -axis, indicating the field selection of antiphase domain.

The cooling-field dependence of $|\bar{\mathbf{n}}|$ qualitatively scales with the spontaneous WFM below 2.5 mT, as shown in Fig. 2(h). In the low-cooling-field region, the magnitude of the spontaneous WFM is attributed to the imbalanced distribution of antiphase domains. However, in the higher-cooling-field region, the imbalance appears to be saturated, whereas the spontaneous WFM continues to increase. In the spontaneous WFM data, a transition point appears around 2.5 mT, and the increase becomes more moderate above this field, which would be related to other mechanism.

The population of one of the orientational domains was further determined from the flipping ratio at a pure magnetic Bragg peak (001) by full-polarized mode with z -polarization, as shown in Fig. 4. In the scattering plane ($h0l$), an ideally balanced distribution of orientational domains, $p_1^+ + p_1^- = p_2^+ + p_2^- = p_3^+ + p_3^-$, leads to $\sigma_y^M = \sigma_z^M$ (see Section VII in SM [52] for details). Thus, the negative $\sigma_y^M - \sigma_z^M$ observed after both ZFC and FC indicates the presence of a natural imbalance in the domain population, $p_1^+ + p_1^- < (p_2^+ + p_2^- + p_3^+ + p_3^-)/2$, as shown in Figs. 4(a), 4(c), and 4(d), possibly caused by defects and local strain in bulk MnTe. The natural imbalance was confirmed by a corresponding measurement with y -

polarization and was found to be common among bulk MnTe samples (see Section IV in SM [52]). σ_y^M increases slightly after OFC, as shown in Fig. 4(b), indicating the increase in $p_1^+ + p_1^-$, which represents the population of \mathbf{n}_1^\pm perpendicular to the oblique cooling field, consistent with the spin-flop configuration.

In conclusion, by using MnTe as an example, we show that PoND serves as a powerful probe of altermagnetic order in a bulk sample, complementing the local detection of magnetic antiphase domains by X-ray dichroism [59], scanning tunneling microscopy [60], and optical methods [61, 62] which are limited to surfaces or thin-film materials. In addition, the method enables sensitive detection of magnetic order in TRS-breaking antiferromagnets, beyond altermagnets such as MnTe₂, thereby promoting research on non-relativistic spin splitting and non-trivial band topology in unconventional antiferromagnets [8, 63, 64].

Our experiments provide direct evidence that the WFM in MnTe is associated with altermagnetic antiphase domains, which can be switched by FC with fields as small as at the milli-Tesla scale. Note that although antiferromagnetic domain walls can give rise to weak ferromagnetism [65], this mechanism is unlikely in bulk MnTe: the observed WFM increases as the magnetic domains become more imbalanced, implying a reduced density of domain walls. WFM is predicted to be widespread in many altermagnets when SOC is included, originating either from spin canting [30, 31] or from orbital ferromagnetism [32]. In addition to MnTe (2×10^{-5} , μ_B/Mn), spontaneous WFM has been observed to accompany altermagnetic order in FeS (5×10^{-4} , μ_B/Fe) [23], Mn₅Si₃ (9×10^{-3} , μ_B/Mn) [66], and CoF₂ (2×10^{-3} , μ_B/Co) [38]. This phenomenon is akin to the spontaneous magnetization arising from non-collinear or non-coplanar antiferromagnetic orders in Mn₃Sn (2×10^{-3} , μ_B/Mn) [4] and CoTa₃S₆ (9×10^{-4} , μ_B/Co) [67], which switch anomalous transport effects. Thus, our findings establish a general

principle for controlling altermagnetic order and open a pathway toward exploring emergent phenomena in altermagnets, such as GMR-like spin-dependent transport effects [68, 69]. Searching for altermagnets with intrinsic WFM, or inducing WFM through doping or strain, will establish a solid foundation for altermagnet-based spintronics applications.

ACKNOWLEDGMENTS

We are grateful to D. Kawana, T. Asami, and R. Sugiyama for their support during the neutron scattering ex-

periments at PONTA. We also acknowledge R. Ishii for assisting with the sample synthesis. The neutron scattering experiments at PONTA, JRR-3, were performed under user program 2025A. The neutron scattering experiment at HODACA, JRR-3 was performed under user program with proposal No. 25403. Z. Liu was supported by the Japan Society for the Promotion of Science (JSPS) through the Program for Leading Graduate Schools (MERIT). This project was supported by JSPS KAKENHI Grant Numbers 21H04441 and 26H02010.

Data availability—The data that support the findings of this article are openly available [70].

-
- [1] Y. Tserkovnyak, A. Brataas, and G. E. W. Bauer, Enhanced Gilbert damping in thin ferromagnetic films, *Phys. Rev. Lett.* **88**, 117601 (2002).
- [2] S. O. Valenzuela and M. Tinkham, Direct electronic measurement of the spin Hall effect, *Nature* **442**, 176 (2006).
- [3] K. Uchida, S. Takahashi, K. Harii, J. Ieda, W. Koshibae, K. Ando, S. Maekawa, and E. Saitoh, Observation of the spin Seebeck effect, *Nature* **455**, 778 (2008).
- [4] M. Kimata, H. Chen, K. Kondou, S. Sugimoto, P. K. Muduli, M. Ikhlas, Y. Omori, T. Tomita, A. H. MacDonald, S. Nakatsuji, and Y. Otani, Magnetic and magnetic inverse spin Hall effects in a non-collinear antiferromagnet, *Nature* **565**, 627 (2019).
- [5] A. Bose, N. J. Schreiber, R. Jain, D.-F. Shao, H. P. Nair, J. Sun, X. S. Zhang, D. A. Muller, E. Y. Tsybal, D. G. Schlom, and D. C. Ralph, Tilted spin current generated by the collinear antiferromagnet ruthenium dioxide, *Nat. Electron.* **5**, 267 (2022).
- [6] R. González-Hernández, L. Šmejkal, K. Výborný, Y. Yahagi, J. Sinova, T. Jungwirth, and J. Železný, Efficient electrical spin splitter based on nonrelativistic collinear antiferromagnetism, *Phys. Rev. Lett.* **126**, 127701 (2021).
- [7] L. Šmejkal, J. Sinova, and T. Jungwirth, Beyond conventional ferromagnetism and antiferromagnetism: a phase with nonrelativistic spin and crystal rotation symmetry, *Phys. Rev. X* **12**, 031042 (2022).
- [8] L.-D. Yuan, Z. Wang, J.-W. Luo, and A. Zunger, Prediction of low- Z collinear and noncollinear antiferromagnetic compounds having momentum-dependent spin splitting even without spin-orbit coupling, *Phys. Rev. Mater.* **5**, 014409 (2021).
- [9] S. Hayami, Y. Yanagi, and H. Kusunose, Momentum-dependent spin splitting by collinear antiferromagnetic ordering, *J. Phys. Soc. Jpn.* **88**, 123702 (2019).
- [10] J. Krempaský, L. Šmejkal, S. W. D'Souza, M. Hajlaoui, G. Springholz, K. Uhlířová, F. Alarab, P. C. Constantinou, V. Strocov, D. Usanov, W. R. Pudelko, R. González-Hernández, A. Birk Hellenes, Z. Jansa, H. Reichlová, Z. Šobáň, R. D. Gonzalez Betancourt, P. Wadley, J. Sinova, D. Kriegner, J. Minár, J. H. Dil, and T. Jungwirth, Altermagnetic lifting of Kramers spin degeneracy, *Nature* **626**, 517 (2024).
- [11] S. Lee, S. Lee, S. Jung, J. Jung, D. Kim, Y. Lee, B. Seok, J. Kim, B. G. Park, L. Šmejkal, C.-J. Kang, and C. Kim, Broken Kramers degeneracy in altermagnetic MnTe, *Phys. Rev. Lett.* **132**, 036702 (2024).
- [12] T. Osumi, S. Souma, T. Aoyama, K. Yamauchi, A. Honma, K. Nakayama, T. Takahashi, K. Ohgushi, and T. Sato, Observation of a giant band splitting in altermagnetic MnTe, *Phys. Rev. B* **109**, 115102 (2024).
- [13] J. Ding, Z. Jiang, X. Chen, Z. Tao, Z. Liu, T. Li, J. Liu, J. Sun, J. Cheng, J. Liu, Y. Yang, R. Zhang, L. Deng, W. Jing, Y. Huang, Y. Shi, M. Ye, S. Qiao, Y. Wang, Y. Guo, D. Feng, and D. Shen, Large band splitting in g -wave altermagnet CrSb, *Phys. Rev. Lett.* **133**, 206401 (2024).
- [14] M. Chilcote, A. R. Mazza, Q. Lu, I. Gray, Q. Tian, Q. Deng, D. Moseley, A.-H. Chen, J. Lapano, J. S. Gardner, G. Eres, T. Z. Ward, E. Feng, H. Cao, V. Lauter, M. A. McGuire, R. Hermann, D. Parker, M.-G. Han, A. Kayani, G. Rimal, L. Wu, T. R. Charlton, R. G. Moore, and M. Brahlek, Stoichiometry-induced ferromagnetism in altermagnetic candidate MnTe, *Adv. Funct. Mater.* **34**, 2405829 (2024).
- [15] B. Jiang, M. Hu, J. Bai, Z. Song, C. Mu, G. Qu, W. Li, W. Zhu, H. Pi, Z. Wei, Y.-J. Sun, Y. Huang, X. Zheng, Y. Peng, L. He, S. Li, J. Luo, Z. Li, G. Chen, H. Li, H. Weng, and T. Qian, A metallic room-temperature d -wave altermagnet, *Nat. Phys.* , 1 (2025).
- [16] F. Zhang, X. Cheng, Z. Yin, C. Liu, L. Deng, Y. Qiao, Z. Shi, S. Zhang, J. Lin, Z. Liu, M. Ye, Y. Huang, X. Meng, C. Zhang, T. Okuda, K. Shimada, S. Cui, Y. Zhao, G.-H. Cao, S. Qiao, J. Liu, and C. Chen, Crystal-symmetry-paired spin-valley locking in a layered room-temperature metallic altermagnet candidate, *Nat. Phys.* , 1 (2025).
- [17] Z. Liu, M. Ozeki, S. Asai, S. Itoh, and T. Masuda, Chiral split Magnon in altermagnetic MnTe, *Phys. Rev. Lett.* **133**, 156702 (2024).
- [18] Q. Sun, J. Guo, D. Wang, D. L. Abernathy, W. Tian, and C. Li, Observation of chiral magnon band splitting in altermagnetic hematite, *Phys. Rev. Lett.* **135**, 186703 (2025).
- [19] R. D. Gonzalez Betancourt, J. Zubáč, R. Gonzalez-Hernandez, K. Geishendorf, Z. Šobáň, G. Springholz, K. Olejník, L. Šmejkal, J. Sinova, T. Jungwirth, S. T. B. Goennenwein, A. Thomas, H. Reichlová, J. Železný, and D. Kriegner, Spontaneous anomalous Hall effect arising from an unconventional compensated magnetic phase in

- a semiconductor, *Phys. Rev. Lett.* **130**, 036702 (2023).
- [20] K. P. Kluczyk, K. Gas, M. J. Grzybowski, P. Skupiński, M. A. Borysiewicz, T. Faş, J. Suffczyński, J. Z. Domagala, K. Graszka, A. Mycielski, M. Baj, K. H. Ahn, K. Výborný, M. Sawicki, and M. Gryglas-Borysiewicz, Coexistence of anomalous Hall effect and weak magnetization in a nominally collinear antiferromagnet MnTe, *Phys. Rev. B* **110**, 155201 (2024).
- [21] H. Reichlova, R. Lopes Seeger, R. González-Hernández, I. Kounta, R. Schlitz, D. Kriegner, P. Ritzinger, M. Lammel, M. Leiviskä, A. Birk Hellenes, K. Olejník, V. Petříček, P. Doležal, L. Horak, E. Schmoranzero, A. Badura, S. Bertaina, A. Thomas, V. Baltz, L. Michez, J. Šinova, S. T. B. Goennenwein, T. Jungwirth, and L. Šmejkal, Observation of a spontaneous anomalous Hall response in the Mn₅Si₃ *d*-wave altermagnet candidate, *Nat. Commun.* **15**, 4961 (2024).
- [22] Z. Zhou, X. Cheng, M. Hu, R. Chu, H. Bai, L. Han, J. Liu, F. Pan, and C. Song, Manipulation of the altermagnetic order in CrSb via crystal symmetry, *Nature* **638**, 645 (2025).
- [23] R. Takagi, R. Hirakida, Y. Settai, R. Oiwa, H. Takagi, A. Kitaori, K. Yamauchi, H. Inoue, J.-i. Yamaura, D. Nishio-Hamane, S. Itoh, S. Aji, H. Saito, T. Nakajima, T. Nomoto, R. Arita, and S. Seki, Spontaneous Hall effect induced by collinear antiferromagnetic order at room temperature, *Nat. Mater.* **24**, 63 (2025).
- [24] A. Hariki, A. Dal Din, O. J. Amin, T. Yamaguchi, A. Badura, D. Kriegner, K. W. Edmonds, R. P. Campion, P. Wadley, D. Backes, L. S. I. Veiga, S. S. Dhessi, G. Springholz, L. Šmejkal, K. Výborný, T. Jungwirth, and J. Kuneš, X-Ray magnetic circular dichroism in altermagnetic α -MnTe, *Phys. Rev. Lett.* **132**, 176701 (2024).
- [25] T. Aoyama and K. Ohgushi, Piezomagnetic properties in altermagnetic MnTe, *Phys. Rev. Mater.* **8**, L041402 (2024).
- [26] M. Roig, A. Kreisel, Y. Yu, B. M. Andersen, and D. F. Agterberg, Minimal models for altermagnetism, *Phys. Rev. B* **110**, 144412 (2024).
- [27] V. Leeb, A. Mook, L. Šmejkal, and J. Knolle, Spontaneous formation of altermagnetism from orbital ordering, *Phys. Rev. Lett.* **132**, 236701 (2024).
- [28] P. A. McClarty and J. G. Rau, Landau theory of altermagnetism, *Phys. Rev. Lett.* **132**, 176702 (2024).
- [29] I. I. Mazin and K. D. Belashchenko, Origin of the gossamer ferromagnetism in MnTe, *Phys. Rev. B* **110**, 214436 (2024).
- [30] C. Autieri, R. M. Sattigeri, G. Cuono, and A. Fakhredine, Staggered Dzyaloshinskii-Moriya interaction inducing weak ferromagnetism in centrosymmetric altermagnets and weak ferrimagnetism in noncentrosymmetric altermagnets, *Phys. Rev. B* **111**, 054442 (2025).
- [31] M. Roig, Y. Yu, R. C. Ekman, A. Kreisel, B. M. Andersen, and D. F. Agterberg, Quasisymmetry-constrained spin ferromagnetism in altermagnets, *Phys. Rev. Lett.* **135**, 016703 (2025).
- [32] D. Jo, D. Go, Y. Mokrousov, P. M. Oppeneer, S.-W. Cheong, and H.-W. Lee, Weak ferromagnetism in altermagnets from alternating *g*-tensor anisotropy, *Phys. Rev. Lett.* **134**, 196703 (2025).
- [33] H. A. Alperin, P. J. Brown, R. Nathans, and S. J. Pickart, Polarized neutron Study of antiferromagnetic domains in MnF₂, *Phys. Rev. Lett.* **8**, 237 (1962).
- [34] G. P. Felcher and R. Kleb, Antiferromagnetic domains and the spin-flop transition of MnF₂, *Europhys. Lett.* **36**, 455 (1996).
- [35] T. Fries, Y. Shapira, A. Paduan-Filho, C. C. Becerra, and F. Palacio, Remanent magnetization of the dilute antiferromagnets Mn_{1-x}Zn_xF₂ at very low magnetic fields, *J. Phys.: Condens. Matter* **5**, 8083 (1993).
- [36] A. S. Disa, M. Fechner, T. F. Nova, B. Liu, M. Först, D. Prabhakaran, P. G. Radaelli, and A. Cavalleri, Polarizing an antiferromagnet by optical engineering of the crystal field, *Nat. Phys.* **16**, 937 (2020).
- [37] H.-Y. Ma, M. Hu, N. Li, J. Liu, W. Yao, J.-F. Jia, and J. Liu, Multifunctional antiferromagnetic materials with giant piezomagnetism and noncollinear spin current, *Nat. Commun.* **12**, 2846 (2021).
- [38] M. Komuro, T. Aoyama, and K. Ohgushi, Revisiting the piezomagnetic effect in the rutile fluorides MnF₂ and CoF₂, *Phys. Rev. B* **111**, 214445 (2025).
- [39] T. Moriya, Anisotropic superexchange interaction and weak ferromagnetism, *Phys. Rev.* **120**, 91 (1960).
- [40] L. M. Sandratskii and J. Kübler, Role of orbital polarization in weak ferromagnetism, *Phys. Rev. Lett.* **76**, 4963 (1996).
- [41] L. Šmejkal, R. González-Hernández, T. Jungwirth, and J. Šinova, Crystal time-reversal symmetry breaking and spontaneous Hall effect in collinear antiferromagnets, *Sci. Adv.* **6**, eaaz8809 (2020).
- [42] P. A. McClarty, A. Gukasov, and J. G. Rau, Observing altermagnetism using polarized neutrons, *Phys. Rev. B* **111**, L060405 (2025).
- [43] R. Nathans, S. J. Pickart, H. A. Alperin, and P. J. Brown, Polarized-neutron study of hematite, *Phys. Rev.* **136**, A1641 (1964).
- [44] M. J. M. de Almeida, Magnetisation density and covalency in ferrous fluoride, *J. Phys. C: Solid State Phys.* **21**, 1111 (1988).
- [45] M. G. Kim, H. Miao, B. Gao, S.-W. Cheong, C. Mazzoli, A. Barbour, W. Hu, S. B. Wilkins, I. K. Robinson, M. P. M. Dean, and V. Kiryukhin, Imaging antiferromagnetic antiphase domain boundaries using magnetic Bragg diffraction phase contrast, *Nat. Commun.* **9**, 5013 (2018).
- [46] H. A. Mook, Magnetic moment distribution of nickel metal, *Phys. Rev.* **148**, 495 (1966).
- [47] K. Prokeš, F. Mezei, and A. Gukasov, Polarized neutron diffraction on a diamagnetic bismuth single crystal, *J. Magn. Magn. Mater.* **485**, 286 (2019).
- [48] J. B. C. Efre D'Sa, P. A. Bhoje, K. R. Priolkar, A. Das, S. K. Paranjpe, R. B. Prabhu, and P. R. Sarode, Low-temperature neutron diffraction study of MnTe, *J. Magn. Magn. Mater.* **285**, 267 (2005).
- [49] Z. Liu, S. Xu, J. M. DeStefano, E. Rosenberg, T. Zhang, J. Li, M. B. Stone, F. Ye, R. Cong, S. Pan, C.-W. Chu, L. Deng, E. Morosan, R. M. Fernandes, J.-H. Chu, and P. Dai, Strain-tunable anomalous Hall effect in hexagonal MnTe (2025), arXiv:2509.19582.
- [50] S. Brinker, M. d. S. Dias, and S. Lounis, The chiral biquadratic pair interaction, *New J. Phys.* **21**, 083015 (2019).
- [51] A. Lászlóffy, L. Rózsa, K. Palotás, L. Udvardi, and L. Szunyogh, Magnetic structure of monatomic Fe chains on Re(0001): Emergence of chiral multispin interactions, *Phys. Rev. B* **99**, 184430 (2019).
- [52] See Supplemental Material at URL for additional information about sample preparation, experimental details, and formulations, which includes Refs. [53–57].

- [53] T. Nakajima, H. Saito, N. Kobayashi, T. Kawasaki, T. Nakamura, H. Kawano-Furukawa, S. Asai, and T. Masuda, Polarized and unpolarized neutron scattering for magnetic materials at the triple-axis spectrometer PONTA in JRR-3, *J. Phys. Soc. Jpn.* **93**, 091002 (2024).
- [54] W. Szuszkiewicz, E. Dynowska, B. Witkowska, and B. Hennion, Spin-wave measurements on hexagonal MnTe of NiAs-type structure by inelastic neutron scattering, *Phys. Rev. B* **73**, 104403 (2006).
- [55] D. Kriegner, H. Reichlova, J. Grenzer, W. Schmidt, E. Ressouche, J. Godinho, T. Wagner, S. Y. Martin, A. B. Shick, V. V. Volobuev, G. Springholz, V. Holý, J. Wunderlich, T. Jungwirth, and K. Výborný, Magnetic anisotropy in antiferromagnetic hexagonal MnTe, *Phys. Rev. B* **96**, 214418 (2017).
- [56] Y. Yu, M. B. Lyngby, T. Shishidou, M. Roig, A. Kreisel, M. Weinert, B. M. Andersen, and D. F. Agterberg, Odd-parity magnetism driven by antiferromagnetic exchange, *Phys. Rev. Lett.* **135**, 046701 (2025).
- [57] B. Brekke, P. Sukhachov, H. G. Giil, A. Brataas, and J. Linder, Minimal models and transport properties of unconventional p -wave magnets, *Phys. Rev. Lett.* **133**, 236703 (2024).
- [58] D. Kriegner, K. Výborný, K. Olejník, H. Reichlová, V. Novák, X. Marti, J. Gazquez, V. Saidl, P. Němec, V. V. Volobuev, G. Springholz, V. Holý, and T. Jungwirth, Multiple-stable anisotropic magnetoresistance memory in antiferromagnetic MnTe, *Nat. Commun.* **7**, 11623 (2016).
- [59] O. J. Amin, A. Dal Din, E. Golias, Y. Niu, A. Zakharov, S. C. Fromage, C. J. B. Fields, S. L. Heywood, R. B. Cousins, F. Maccherozzi, J. Krempaský, J. H. Dil, D. Kriegner, B. Kiraly, R. P. Campion, A. W. Rushforth, K. W. Edmonds, S. S. Dhesi, L. Šmejkal, T. Jungwirth, and P. Wadley, Nanoscale imaging and control of altermagnetism in MnTe, *Nature* **636**, 348 (2024).
- [60] U. Kaiser, A. Schwarz, and R. Wiesendanger, Magnetic exchange force microscopy with atomic resolution, *Nature* **446**, 522 (2007).
- [61] A. Scholl, J. Stöhr, J. Lüning, J. W. Seo, J. Fompeyrine, H. Siegwart, J.-P. Locquet, F. Nolting, S. Anders, E. E. Fullerton, M. R. Scheinfein, and H. A. Padmore, Observation of antiferromagnetic domains in epitaxial thin films, *Science* **287**, 1014 (2000).
- [62] M. Fiebig, D. Fröhlich, B. B. Krichevstov, and R. V. Pisarev, Second harmonic generation and magnetic-dipole-electric-dipole interference in antiferromagnetic Cr_2O_3 , *Phys. Rev. Lett.* **73**, 2127 (1994).
- [63] L.-D. Yuan, A. B. Georgescu, and J. M. Rondinelli, Non-relativistic spin splitting at the Brillouin zone center in compensated magnets, *Phys. Rev. Lett.* **133**, 216701 (2024).
- [64] X. Chen, Y. Liu, P. Liu, Y. Yu, J. Ren, J. Li, A. Zhang, and Q. Liu, Unconventional magnons in collinear magnets dictated by spin space groups, *Nature* **640**, 349 (2025).
- [65] M. Bode, E. Y. Vedmedenko, K. von Bergmann, A. Kubetzka, P. Ferriani, S. Heinze, and R. Wiesendanger, Atomic spin structure of antiferromagnetic domain walls, *Nature Mater* **5**, 477 (2006).
- [66] A. Badura, W. H. Campos, V. K. Bharadwaj, I. Kounta, L. Michez, M. Petit, J. Rial, M. Leiviskä, V. Baltz, F. Krizek, D. Kriegner, J. Železný, J. Zemen, S. Telkamp, S. Sailler, M. Lammel, R. Jaeschke-Ubiergo, A. B. Hellenes, R. González-Hernández, J. Sinova, T. Jungwirth, S. T. B. Goennenwein, L. Šmejkal, and H. Reichlova, Observation of the anomalous Nernst effect in altermagnetic candidate Mn_5Si_3 , *Nat. Commun.* **16**, 7111 (2025).
- [67] H. Takagi, R. Takagi, S. Minami, T. Nomoto, K. Ohishi, M.-T. Suzuki, Y. Yanagi, M. Hirayama, N. D. Khanh, K. Karube, H. Saito, D. Hashizume, R. Kiyonagi, Y. Tokura, R. Arita, T. Nakajima, and S. Seki, Spontaneous topological Hall effect induced by non-coplanar antiferromagnetic order in intercalated van der Waals materials, *Nat. Phys.* **19**, 961 (2023).
- [68] L. Šmejkal, A. B. Hellenes, R. González-Hernández, J. Sinova, and T. Jungwirth, Giant and tunneling magnetoresistance in unconventional collinear antiferromagnets with nonrelativistic spin-momentum coupling, *Phys. Rev. X* **12**, 011028 (2022).
- [69] S. Noh, G.-H. Kim, J. Lee, H. Jung, U. Seo, G. So, J. Lee, S. Lee, M. Park, S. Yang, Y. S. Oh, H. Jin, C. Sohn, and J.-W. Yoo, Tunneling magnetoresistance in altermagnetic RuO_2 -Based magnetic tunnel junctions, *Phys. Rev. Lett.* **134**, 246703 (2025).
- [70] Z. Liu, S. Asai, S. Takahashi, H. Saito, T. Nakajima, and T. Masuda, Observation of Altermagnetic Order Switching in Bulk MnTe by Polarized Neutron Diffraction, *Zenodo* (2026), 10.5281/zenodo.20305737.